Revista Minelor – Mining Revue
ISSN-L 1220-2053 / ISSN 2247-8590
vol. 32, issue 2 / 2026, pp. 132-148

OPTIMISATION MODELLING OF RESERVOIR PROPERTIES – A COMPARATIVE STUDY BETWEEN HYDRODYNAMIC AND GEOPHYSICAL INVESTIGATIONS

Dragoş CRISTEA [1], Iulia VASILIU [2], Iulian NISTOR [3], Timur CHIS [4]*

[1]Oil and Gas Engineering Faculty, Petroleum-Gas University Ploiesti, Romania, dragos.cristea@upg-ploiesti.ro
[2]Ph.D School, Petroleum-Gas University Ploiesti, Romania, svasiliu_iulia@yahoo.com
[3]Oil and Gas Engineering Faculty, Petroleum-Gas University Ploiesti, Romania, nistor@upg-ploiesti.ro
[4]Oil and Gas Engineering Faculty, Petroleum-Gas University Ploiesti, Romania, timur.chis@gmail.com

DOI: 10.2478/minrv-2026-0020
received – 20.04.2026 / revised – 04.05.2026
accepted – 03.06.2026 / published – 19.06.2026

Abstract: *This research addresses the critical challenge of reconciling reservoir permeability values derived from two distinct methods: Geophysical Well Logging and Hydrodynamic Pressure Transient Analysis (PTA). While geophysical methods provide high-resolution vertical data, they often overestimate permeability due to formation damage and filtrate invasion. Conversely, hydrodynamic testing yields effective permeability reflecting true flow capacity but lacks vertical detail. This study calculates key gas properties (density, viscosity, and Z-factor) to perform a pressure build-up analysis, revealing a significant discrepancy between the measured effective permeability (4.67mD) and log-derived estimates (up to 140.225 mD). The primary contribution is the development of an optimized mathematical model that integrates shale volume (Vsh) to calibrate geophysical logs against real-world hydrodynamic performance.*
Keywords: *porosity, permeability, geophysics, hydrodynamic investigations, lithology log, skin factor*

1. Introduction

The accurate determination of petrophysical parameters, particularly permeability and porosity, remains a cornerstone of effective reservoir management and production optimization, [1].

In modern petroleum engineering, this characterization relies on a multi-disciplinary approach, predominantly integrating Geophysical Well Logging and Hydrodynamic Pressure Transient Analysis (PTA).

However, recent research studies have highlighted a persistent challenge: the "scale-dependency" and "methodological bias" in permeability estimation, [2].

While geophysical logs provide a continuous vertical profile of the formation's physical properties, they represent a "static" snapshot of the near-wellbore area, often affected by filtrate invasion and mud cake buildup. In contrast, hydrodynamic tests provide a "dynamic" measurement of the reservoir's flow capacity over a much larger drainage area, yet they yield a single averaged value for the entire tested interval, [3].

Recent research trends [4] and Al-Khalifah [5] on the integration of scale-dependent data) emphasize that the discrepancy between these two methods is not merely an error, but a reflection of reservoir heterogeneity and formation damage. For instance, in shaly-sandstone reservoirs—similar to the Sarmatian formations analysed in this paper—the presence of clay minerals significantly complicates log interpretation, leading to overestimations of effective permeability in traditional models like Coates or Timur, [6].

This study builds upon these research foundations by performing a comparative analysis of a gas well.

We investigate the calculation of key gas properties (density, viscosity, and Z-factor) as a prerequisite for rigorous PTA. The novelty of this work lies in the development of a hybrid optimization model. By using the hydrodynamic "ground truth" to calibrate geophysical empirical relations through non-linear regression, we

* Corresponding author: Chiș Timur, assoc.prof. Ph.D. eng., Oil and Gas Engineering Faculty, Petroleum-Gas University Ploiesti, Romania, Contact details: etroleum-Gas University Ploiesti, 39 Bucharest Boulevard, timur.chis@gmail.com

vol. 32, issue 2 / 2026
pp. 132-148

propose a more reliable framework for predicting effective permeability in complex lithologies, accounting for the Skin Factor (s) and Shale Volume (V_{sh}) as primary corrective variables.

In reservoir engineering, accurate determination of reservoir parameters is essential for estimating hydrocarbon resources and evaluating the production potential of a reservoir.

In this study, reservoir parameters are determined using two complementary approaches: geophysical investigations and hydrodynamic well testing.

The main parameters analysed are porosity, permeability, and irreducible water saturation, which are fundamental for reservoir characterization and for evaluating the storage and flow capacity of hydrocarbon reservoirs.

Using these parameters, additional quantities of interest for hydrocarbon reservoirs will be calculated.

The purpose of this work is to identify the investigation methods that provide the highest measurement accuracy and to determine ways in which these methods can be improved.

2. Materials and method

The research methodology follows a comparative and integrative workflow designed to reconcile static geophysical measurements with dynamic reservoir performance.

This approach is divided into two primary phases: hydrodynamic pressure transient analysis and petrophysical log interpretation. The hydrodynamic parameters were determined through a pressure build-up test conducted on the subject gas well. The methodology for this phase includes the analysis of production history (the well was produced at a constant flow rate of 9,500 m^3/day for a duration of 200 hours to establish a stable drainage area before shut-in and a Build-up Test (following production, the well was shut in for 21.5 hours, during which pressure data was recorded, increasing from 90.547 bar to 95.353 bar).

The Gas Property Modelling analysis a density, viscosity, compressibility factor (Z-factor), and the formation volume factor were calculated.

Pseudo-pressure Determination (u) is a pressure-dependent nature of gas properties, the analysis utilized the pseudo-pressure function to linearize the flow equations.

A Horner-style plot of pseudo-pressure versus is using to analysis $\log(t + \Delta t)$ was generated to determine the slope (i), which is essential for calculating formation flow capacity (kh) and effective permeability (k).

In the final analysis, the skin factor (s) was calculated to quantify near-wellbore damage, and the storage coefficient (C) was determined using a log-log plot to account for wellbore storage effects during the early stages of the test.

Accurate reservoir characterization is fundamental for resource estimation and production forecasting. This study focuses on a gas reservoir where porosity, permeability, and water saturation are analysed through a dual-investigation approach. The objective is to identify the sources of measurement error—such as the Skin Effect and lithological variations—and to propose a unified modelling technique to improve the reliability of reservoir parameter. The studied well was subjected to a pressure build-up test lasting 21.5 hours, and the resulting data are presented in Table 1. Prior to shut-in, the well was produced at a constant flow rate of 9500 m^3/day for 200 hours.

Table 1. Data obtained from the pressure build-up test

Δt	$tp+\Delta t$	**Pressure**
hours	hours	bar
0	200	90.547
0.5	200.5	91.381
1.5	201.5	93.0582
2.5	202.5	94.0389
3.5	203.5	94.7351
5.5	205.5	95.01957
8,5	208.5	95.0882
21.5	221.5	95.353

In parallel, geophysical logs provided a high-resolution vertical characterization of the reservoir, to analyse porosity Modelling (In the absence of modern porosity logs, the "Maximum Porosity" method (Material Balance for Porosity) was applied using a PHIMAX of 35% calibrated against core data and Neutron-Density crossplots were utilized to differentiate lithology and determine the shale volume (Vsh) and effective porosity (ϕ_e).

Absolute permeability was initially estimated using the Tixier, Timur, and Coates equations, which yielded average values of 7.58 mD, 15.64 mD, and 140.225 mD, respectively.

To resolve the discrepancies between the methods, an optimization framework was implemented; the data processing was facilitated by the Petrophysical Interpretation Software (for log analysis and crossplots) and Pressure Transient Analysis (PTA) Software (for Horner plots and storage factor calculation); a non-linear regression model was developed by assigning shale volume values from 5% to 35% and calculating the corresponding effective permeability.

The final step involved merging the empirical Tixier, Timur, and Coates, [7,8,9] relations with the derived variation curves to create a new calculation relationship for permeability as a function of porosity, water saturation, and shale volume.

The hydrodynamic characterization began with the analysis of raw data collected during the well's transition from production to shut-in.

Figure 1 illustrates the variation of the flow rate and pressure throughout the duration of the well shut-in test.

Before the test, the well maintained a constant flow rate of 9500 m^3/day for a period of 200 hours.

Upon shut-in, a rapid pressure recovery is observed, increasing from a flowing bottom-hole pressure of approximately 90.5 bar toward a stabilized reservoir pressure of 95.35 barover the 21.5 hours build-up period.

To account for the non-linear behaviour of gas under varying pressures, the study utilized the pseudo-pressure approach.

The relationship between pressure and the term $(2p/(Z \cdot \mu_g)$which incorporates the gas compressibility factor (Z) and viscosity (μ_g)—is detailed in Figure 2.

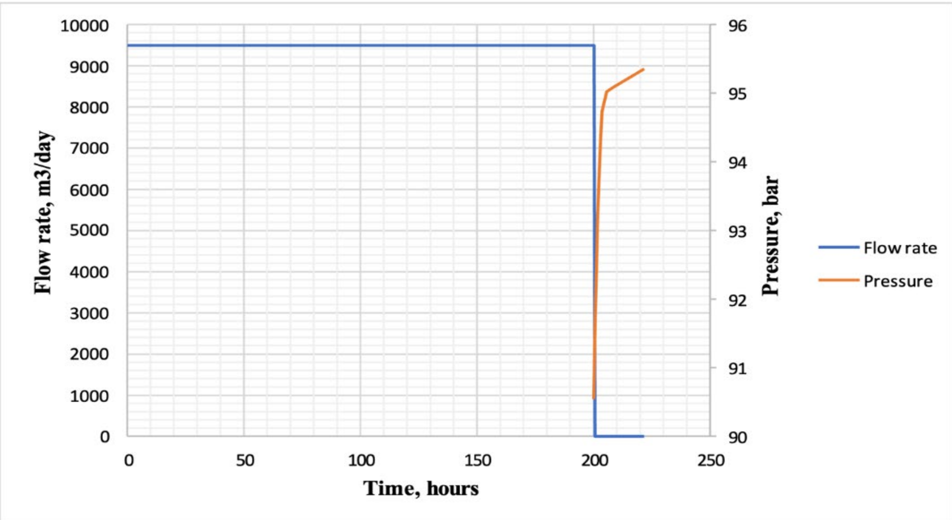

Fig. 1. Variation of flow rate and pressure during the well shut-in test

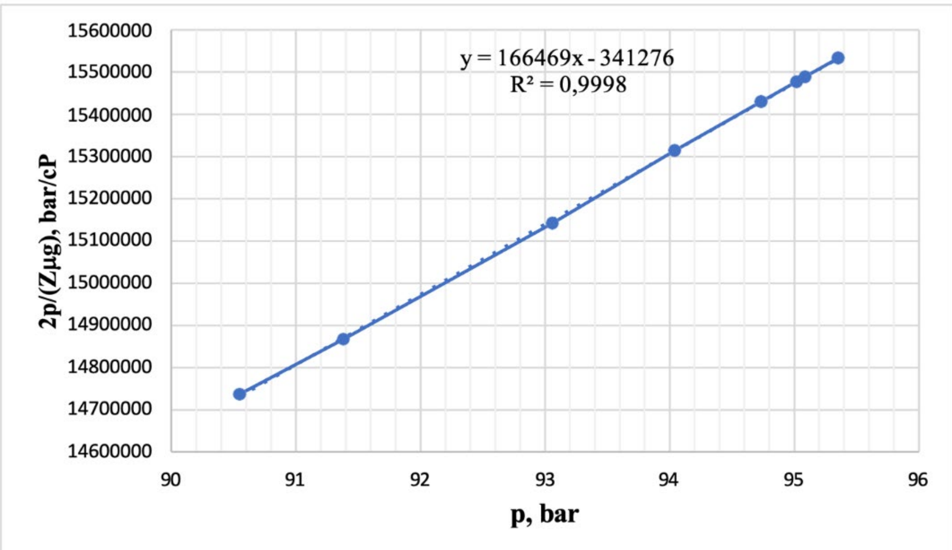

Fig. 2. Variation of the parameter 2p/(Z·μg) as a function of pressure

vol. 32, issue 2 / 2026
pp. 132-148

This plot (R^2=0,9998) is use to serves as the mathematical foundation for calculating the precise pseudo-pressure values (u) required for the Horner plot analysis ($y = 166469\,x - 341276$).

To accurately analyse gas well performance, the pressure-dependent variations of gas properties must be accounted for. Table 2 summarizes the calculation of the pseudo-pressure (u), which integrates the effects of pressure (p), gas viscosity μ_g), and the compressibility factor (Z).

Table 2. Pseudo-pressure determination

Pressure	p_{pr}	μ_g	***Z***	***2p/(Z μg)***	***u***
bar	-	cP	-	bar/cP	bar^2/cP
90.547	1.927803445	0.013365	0.919398	14737.69	667226.6723
91.381	1.945559837	0.013372	0.919286	14867.7	679312.4447
93.0582	1.981268496	0.013384	0.918315	15142.29	704556.9439
94.0389	2.002148225	0.013391	0.917102	15314.37	720073.3257
94.7351	2.016970768	0.013396	0.916653	15430.13	730887.2238
95.01957	2.023027316	0.013398	0.91647	15477.5	733582.8696
95.0882	2.024488492	0.013398	0.916426	15488.94	736407.7643
95.353	2.030126253	0.0134	0.916256	15533.1	740563.7142

Table 3 organizes the data into the semi-logarithmic format necessary for the Horner Plot, and these values are plotted against pseudo-pressure (u) to determine the straight-line slope (i), which was calculated as -11,031 Pa/cycle.

This slope is the fundamental variable used to derive the effective permeability of 4.67 mD.

Next, using a **semi-logarithmic plot**, the variation of **pseudo-pressure** as a function of **log((*t+Δt)/t*)** will be examined.

Table 3. Pseudo-pressure variation

u	***(t+dt)/dt***	***log((t+dt)/dt)***
bar^2/cP	-	-
667226.6723	-	-
679312.4447	401	2.603144373
704556.9439	134.3333333	2.128183791
720073.3257	81	1.908485019
730887.2238	58.14285714	1.764496369
733582.8696	37.36363636	1.572449137
736407.7643	24.52941176	1.389687134
740563.7142	10.30232558	1.012935271

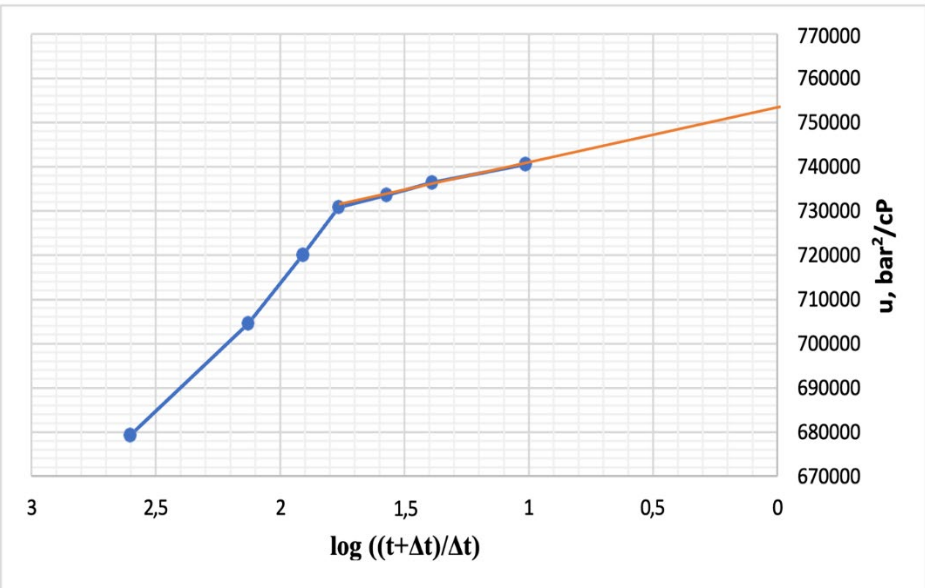

Fig. 3. Semi-logarithmic variation of the pseudo-pressure as a function of log((t+Δt)/t)

Revista Minelor – Mining Revue
ISSN-L 1220-2053 / ISSN 2247-8590
vol. 32, issue 2 / 2026
pp. 132-148

From the graph shown in Figure 3, the *apparent initial pseudo-pressure*, u^*, and the *pseudo-pressure at* $\Delta t = 1$ *hour* are determined.

$$u^* = 752000\ bar^2/cP$$

$$u_{\Delta t=1\ or\breve{a}} = 692000\ bar^2/cP$$

The *slope of the line*, i, is calculated.

$$i = \frac{736407.7643-740563.7142}{1.3896-1.0129} = -11031\ Pa/cycle \tag{1}$$

Next, the *formation flow capacity* is calculated, from which the *effective permeability* can also be determined.

$$kh = \frac{2{,}3Q\mu b}{4\pi|i|} = \frac{2.3\cdot 0.109954\cdot 345.15\cdot 101325}{4\ \pi\cdot 273.15\cdot 11031\cdot 10^{13}} = 4.67\cdot 10^{-14}\,m^2\cdot m \tag{2}$$

$$k = \frac{kh}{h} = \frac{4.67\cdot 10^{-14}}{10} = 4.67\cdot 10^{-15}\ m^2 = 4.67\ mD \tag{3}$$

The skin factor can be determined using:

$$s = 1.151\cdot\left(\frac{p_{\Delta t=1hour}-p_{\Delta=0}}{|i|} - \log\frac{k}{m\cdot\mu\cdot\beta_T\cdot r_s^2} - 0.351\right) = 1.151\cdot$$

$$\left(\frac{692000-667226.6723}{11031} - \log\frac{4.67\cdot 10^{-15}}{0.18\cdot 0{,}013396\cdot 10^{-13}\ 0.00779\cdot 0{,}1^2} - 0.351\right) = 1.7254 \tag{4}$$

A *damage zone exists around the wellbore*, with a damage value of **27%**.

The *additional pressure drop due to the skin factor* is calculated using the following relation:

$$\Delta u_s = 0.87\cdot s\cdot|i| = 0.87\cdot 1.7254\cdot 11031 = 16559.34\ bar^2\ /\ \text{cP} \tag{5}$$

The productivity ratio is given by:

$$RP = \frac{(IP)_r}{(IP)_i} = 1 - \frac{\Delta u_s}{u^*-u_{\Delta t=0}} = 1 - \frac{16559.34}{752000-667226.67} = 0{,}8046 \tag{6}$$

The mobility is calculated using the following relation:

$$\lambda = \frac{k}{\mu} = \frac{4.67}{0.013396} = 348.73\,\frac{mD}{cP} \tag{7}$$

To calculate the *storage factor*, the variation $\log u = f(\log(\Delta t))$will be plotted. After the plot is obtained, the coordinates of a point from the *linear region with unit slope* will be read (figure 4).

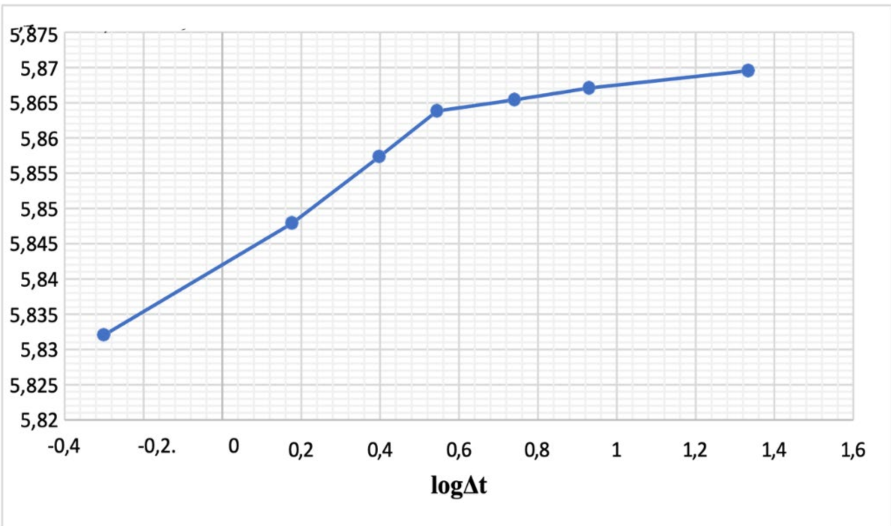

Fig. 4. Variation of $\log u = f(\log(\Delta t))$

The following coordinates are obtained from the graph:

$$log\ u = 5.8675 \Longrightarrow u = 737904.2\ bar^2/cP \Longrightarrow p = 95.12\ bar \tag{8}$$

$$log\ \Delta t = 1.1 \Longrightarrow \Delta t = 12.6\ \text{hours} \tag{9}$$

The *storage factor* is:

$$C = \frac{Q\ b\ \Delta t}{\Delta p} = \frac{0.19954\cdot 12.6\cdot 3600}{95.12} = 0.33\,\frac{m^3}{bar} \tag{10}$$

Revista Minelor – Mining Revue
ISSN-L 1220-2053 / ISSN 2247-8590
vol. 32, issue 2 / 2026
pp. 132-148

The radius of investigation is calculated using relation:

$$r_{inv} = \sqrt{\frac{4 \cdot k \cdot \Delta t}{m \cdot \mu \cdot \beta_T}} = \sqrt{\frac{4 \cdot 4.67 \cdot 10^{-15} \cdot 21.5 \cdot 3600}{0.18 \cdot 0.013396 \cdot 10^{-3} \cdot 0.00779 \cdot 10^{-5}}} = 87.74\, m \qquad (11)$$

3. Discussion

Since porosity logs are unavailable, the "Maximum Porosity" method (Material Balance for Porosity) was used to determine porosity, [8]:

$$P_{hie} = PHIMAX \cdot (1 - V_{sh}) \qquad (12)$$

where the maximum porosity value, PHIMAX = 35%, is obtained from core samples and data from correlation wells.

This value was recorded in clean sand and was adopted from a previous study. Ideally, the porosity obtained through this method should be calibrated with core measurements or with porosity values from correlation wells that possess core data or modern porosity logs.

To determine the permeability, the Timur equation was used, [9]:

$$Perm_{Timur} = kw \cdot \frac{PHI^d}{SW^e} \qquad (13)$$

where: d=4.4, e=2, kw=340 for gas.

The estimation of porosity was carried out using a combination of density and neutron logs.

The sonic log was not utilized due to the high porosity of the rocks, where there is a weak dependence on porosity and where the effects produced by gas/oil are entirely unpredictable.

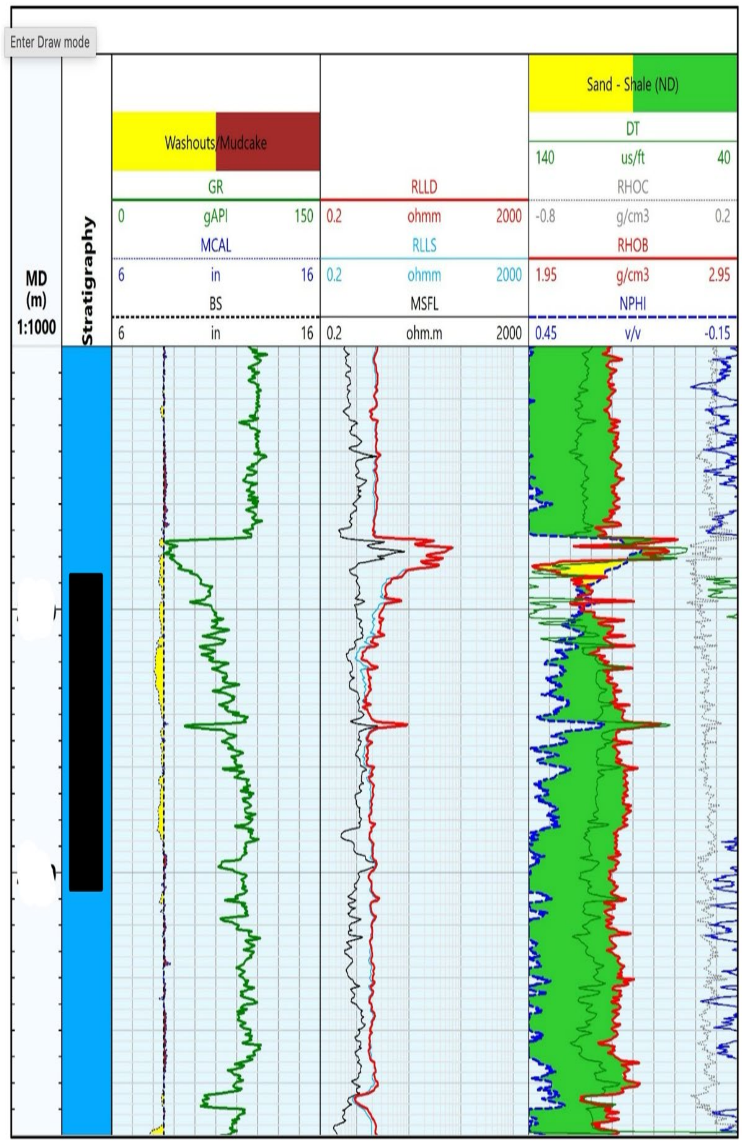

Fig. 5. Complex logs – overlay diagram

Revista Minelor – Mining Revue
ISSN-L 1220-2053 / ISSN 2247-8590
vol. 32, issue 2 / 2026
pp. 132-148

Figure 5 describes complex Geophysical Logs (Overlay Diagram); Track 1 (Lithology) is a Displays the Gamma Ray (GR) and Caliper (MCAL) logs to identify clean sand intervals versus shale-rich zones, Track 2 (Resistivity) is a Shows deep (RLLD) and shallow (RLLS) resistivity curves, which are used to detect hydrocarbon presence and filtrate invasion zones and Track 3 (Porosity/Density) is a features an overlay of Neutron Porosity (NPHI) and Bulk Density (RHOB). The "crossover" between these curves is a classic indicator of gas-bearing sandstone.

Figure 6 visualizes the continuous interpretation results, specifically the vertical distribution of permeability, the log identifies specific intervals, such as "marly sand" and "gas-bearing" zones and displays the PERM_Timur curve, showing how permeability fluctuates with depth.

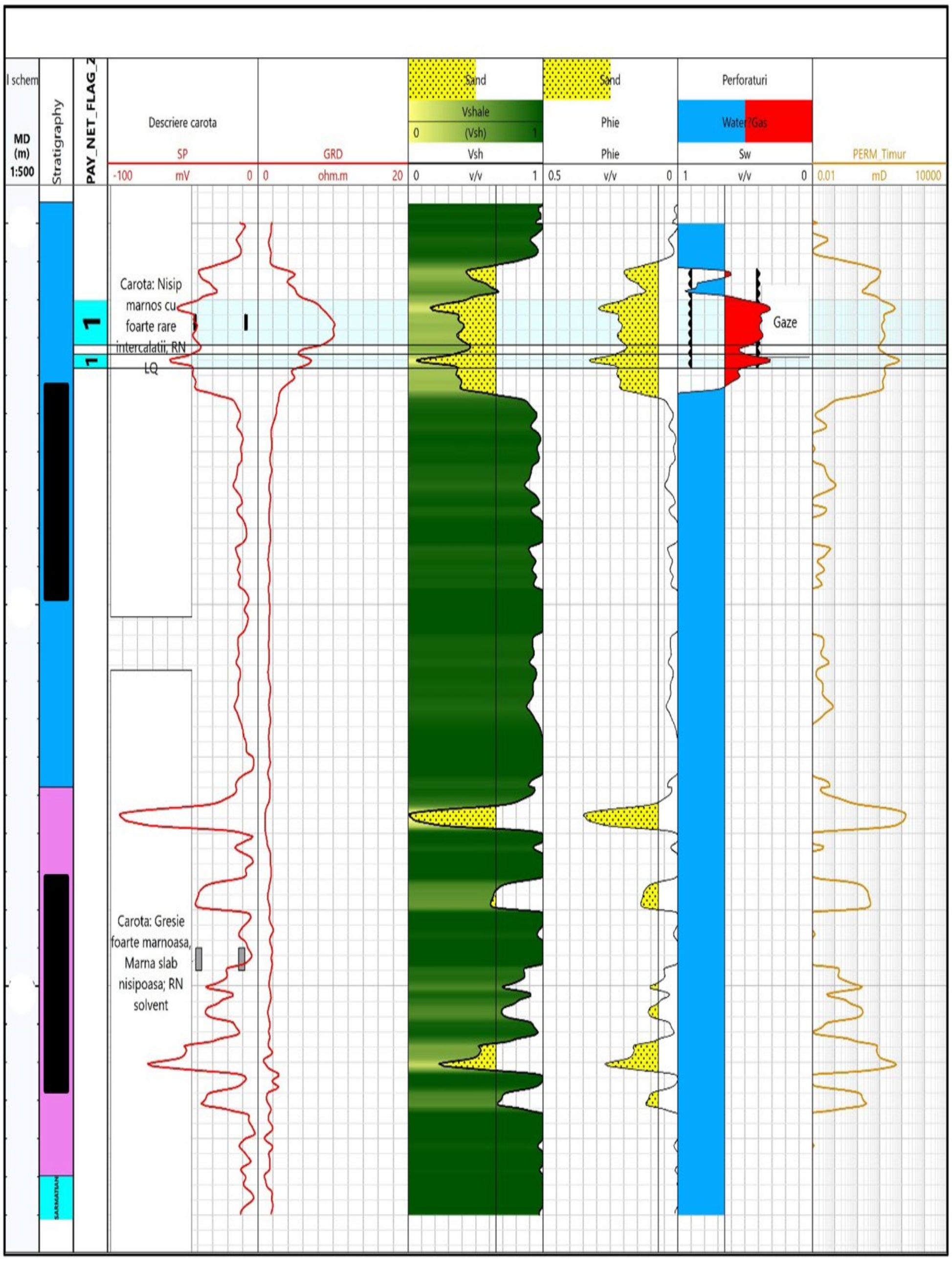

Fig. 6. Permeability from logs

Figure 7 presents the Density-Neutron crossplot used in the interpretation.

The values read from the geophysical logs were recorded in Table 4. Using these values and applying the relations of Tixier, Timur and Coates, the effective permeability of the reservoir was calculated (Table 5).

$$k^{1/2} = 250 \cdot \frac{PHI^3}{S_{wi}} \quad Tixier \tag{14}$$

vol. 32, issue 2 / 2026
pp. 132-148

$$k^{1/2} = 100 \cdot \frac{PHI^{2,25}}{S_{wi}} \quad Timur \tag{15}$$

$$k^{1/2} = 70 \cdot \frac{PHI^{2} \cdot (1-S_{wi})}{S_{wi}} \quad Coates \tag{16}$$

The average permeability scores obtained with the help of the three equations are:

$$\boldsymbol{k_{Tix_m} = 7.58\ mD}$$

$$\boldsymbol{k_{Tim_m} = 15.64\ mD}$$

$$\boldsymbol{k_{Co_m} = 140.225\ mD}$$

Analysing Coates & Dumanoir relationship, following the successive processing steps presented below, it is observed that the only way to determine the coefficient is by assigning random values to it until the resulting permeability matches the desired value.

$$k = \frac{900}{w^8} \frac{\phi^{2w}}{S_{wi}^{2w}} \tag{17}$$

$$\ln k = \ln\left(\frac{900}{w^8}\left(\frac{\phi}{S_{wi}^{2w}}\right)^{2w}\right) \tag{18}$$

$$\ln k = \ln\frac{900}{w^8} + 2w\ln\left(\frac{\phi}{S_{wi}}\right) \tag{19}$$

This track highlights the core problem while the logs show high-permeability "peaks" in clean sands, the hydrodynamic test provides a much lower, averaged effective permeability for the entire interval (table 4).

Table 4. Analysis of the data to figure 5

Feature	Parameter	Source/Result
Wellbore Storage	Storage Factor (*C*)	0.33 m^3/bar
Gas Identification	NPHI/RHOB Crossover	Observed in Fig. 5
Log Permeability	Average (k_Timur)	15.64 mD

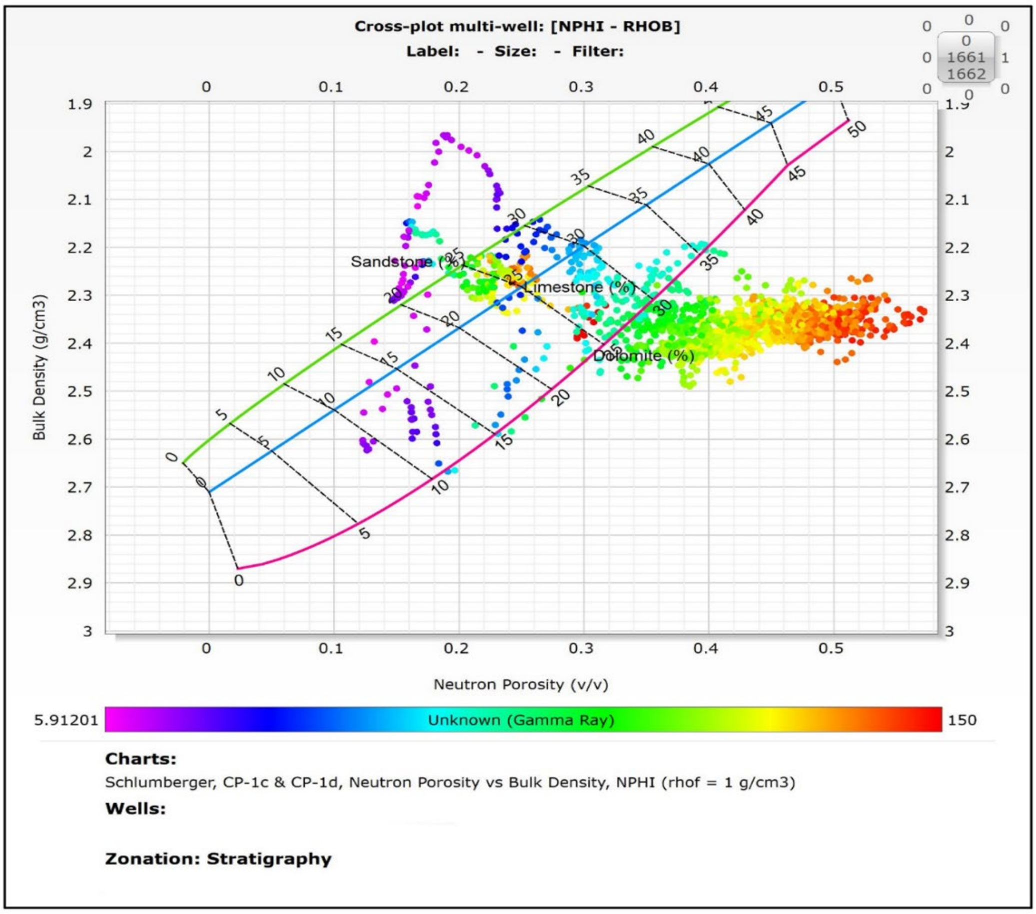

Fig. 7. Porosity from Neutron-Density crossplot

vol. 32, issue 2 / 2026
pp. 132-148

Table 5 presents the essential petrophysical data derived from the interpretation of geophysical logs for the analysed depth interval. This table serves as the primary dataset for calculating permeability and for developing the optimized mathematical models proposed in the study. The fluctuations of Heterogeneity in V_{sh} and ϕ_e recorded in Table 5 highlight the lithological complexity of the reservoir, specifically the transitions between clean sandstone and marly sand.

Permeability Equations are measurements were used as the input variables for the Tixier, Timur, and Coates empirical formulas.

The data in Table 5 provided the foundation for the non-linear regression analysis. By assigning Vsh values from this table (ranging from 5% to 35%), the researchers were able to derive the new hybrid equations that reconcile geophysical data with hydrodynamic "ground truth".

Table 5. Porosity, Water saturation and Shale volume from geophysical logs

Depth	Neutron Porosity *(N)*	Shale Volume *Vsh*	Effective Porosity ϕ_e	Water Saturation S_w
m	-	-	-	-
2354	0.25	0.38	0.15	0.52
2355	0.21	0.07	0.16	0.46
2356	0.33	0.08	0.19	0.5
2357	0.3	0.4	0.18	0.5
2358	0.27	0.35	0,.9	0.45
2359	0.27	0.42	0.16	0.56
2360	0.29	0.48	0.18	0.75
2361	0.27	0.5	0.21	0.78
2362	0.3	0.49	0.19	0.65
2363	0.36	0.52	0.19	0.6
2364	0.27	0.47	0.17	0.35
2365	0.25	0.46	0.18	0.5
2366	0.26	0.47	0.19	0.6
2367	0,24	0.6	0.17	0.68
2368	0.21	0.5	0.14	0.55
2369	0.28	0.49	0.15	0,6
2370	0.34	0.48	0.18	0.67
2371	0.36	0.35	0.2	0.61
2372	0.34	0.41	0.17	0.49
2373	0.34	0.3	0.185	0.49
2374	0.35	0.32	0.175	0.38
2375	0.36	0.3	0.19	0.4
2376	0,33	0.45	0.195	0.5
2377	0.28	0.3	0.16	0.51
2378	0.2	0.32	0.14	0.6
2379	0.35	0.31	0.18	0.6

Figure 7 analysis a porosity from Neutron-Density Crossplot. This crossplot is a fundamental petrophysical tool used to determine both lithology and porosity simultaneously.

The plot displays a cloud of points representing the reservoir interval, positioned between the sandstone and limestone lines and Gas Effect is **a** noticeable shift of data points toward the upper left (lower density, lower neutron porosity) confirms the presence of gas, as gas in the pores lowers the bulk density while significantly reducing the neutron porosity reading (the "gas effect").

Porosity Determination is based on this crossplot and the "Maximum Porosity" method, an effective porosity (ϕ_e) was determined for each depth interval, ranging from 0.14 to 0.21

After several trials, the values for were established, for which the calculated permeability matches the value resulting from the geophysical logs (Table 7).

Furthermore, due to the significant discrepancy between the values calculated using geophysical methods and the permeability value calculated based on pressure transient analysis (PTA) data (build-up test),

I recalculated the multiplication coefficients for the three permeability calculation relations Tixier, Timur, and Coates, so that the permeability values resulting from both methods are equal.

The results are recorded in Table 7.

vol. 32, issue 2 / 2026
pp. 132-148

Table 6. Permeability from the three equations (Tixier, Timur and Coates)

Depth	k_{Tix}	k_{Tim}	k_{Co}
m	mD	mD	mD
2354	2.63282	7.2511	93.9408
2355	4.95546	12.3887	172.865
2356	11.7615	22.7222	176.89
2357	8.50306	17.815	158.76
2358	14.5203	28.0522	264.243
2359	3.34367	8.35918	77.44
2360	3.77914	7.91779	17.64
2361	8.81062	14.6487	17.1906
2362	6.95945	13.4451	51.2876
2363	8.16769	15.7793	78.6178
2364	12.3151	28.1115	488.41
2365	8.50306	17.815	158.76
2366	8.16769	15.7793	78.6178
2367	3.26254	7.44736	31.36
2368	1.55569	4.75172	64.2912
2369	1.97754	5.44638	49
2370	4.7355	9.92148	38.5141
2371	10,7498	19.2298	80.1172
2372	6.28321	14.3426	153.406
2373	10.4356	20.9836	181.672
2374	12.432	27.1709	399.474
2375	18.3773	35.5035	398.003
2376	13.7451	25.5397	186.323
2377	4.03143	10.0786	115.794
2378	1.30721	3.99276	42.6844
2379	5.9049	12.3715	70.56

Given that the shale volume present in this reservoir is quite high, and its influence on permeability values is significant, we sought a direct relationship between permeability and clay volume, starting from the equations of Tixier, Timur, and Coates.

To achieve this, we followed several steps:

1. We assigned values to the shale volume ranging from 5% to 35% and calculated the effective porosity corresponding to these shale volume values.
2. Based on the Tixier, Timur, and Coates relations, we calculated the effective permeability values characteristic of the previously determined porosity values. We then plotted them in a diagram, assuming an average water saturation (Figures 8-10).
3. By combining the Tixier, Timur, and Coates relations with the equations characteristic of the permeability variation curves as a function of shale volume, we obtained a direct relationship between permeability and clay volume.

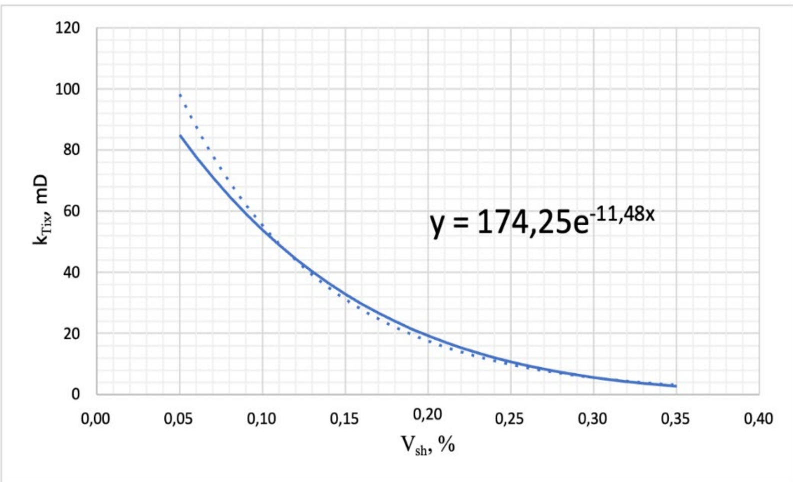

Fig. 8. Permeability vs Shale volume - Tixier

 vol. 32, issue 2 / 2026
pp. 132-148

The equation that describes the variation of permeability with the shale volume when using the Tixier equation is:

$$k = 174.25 \cdot e^{-11.48 \cdot V_{sh}} \quad (20)$$

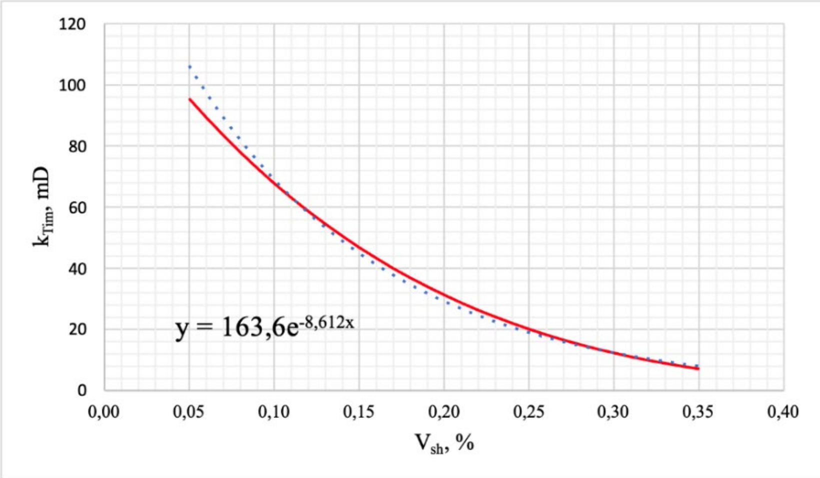

Fig. 9. Permeability vs Shale volume - Timur

Figure 8 illustrates the non-linear relationship between permeability (k_{Tix}) and shale volume (V_{sh}) specifically derived using the Tixier empirical relationship and he plot demonstrates that as the clay content increases within the reservoir rock, the flow capacity decreases drastically. For instance, at a low shale volume of 5% (0.05), the estimated permeability is near 85 mD, but it drops to approximately 3 mD as the shale volume reaches 35% (0.35).

This figure was essential for creating the study's Hybrid Optimization Model.

By combining this characteristic curve with the hydrodynamic "ground truth" (k_{hyd} = 4.67 mD), the researchers derived the final optimized formula for this specific reservoir:

$$k = 0.5\, k_0 + 87.125\, e^{-11{,}48\, V_{sh}} \quad (21)$$

În equation 21 $k_0$is original permeability value calculated using the standard empirical geophysical equations (Tixier, Timur, or Coates) before any hydrodynamic calibration is applied.

In the proposed general formula,

$$k = a\, k_0 + b\, e^{-c\, V_{sh}} \quad (22)$$

the term $a\, k_0$ acts as the base geophysical input.

The optimization process uses this value in conjunction with the shale volume (V_{sh}) to anchor the final result to the "ground truth" established by the hydrodynamic pressure transient analysis.

The paper specifically applies k_0 to adjust the scale of the log-derived data to match the measured effective permeability of 4.67 mD, [10, 11, 12]:

- For the Tixier-based model k_0 refers to the permeability calculated by the standard Tixier equation ($k_{Tixm} = 7.58\, mD$)
- For the Timur-based model k_0 refers to the value from the standard Timur equation ($k_{Timm} = 15{,}56\, mD$)
- For the Coates-based model $k_0$refers to the value from the standard Coates equation ($k_{Ticm} = 140.225\, mD$).

By using a multiplier (*a* = 0.5) for $k_0$the model compensates for the Skin Factor (s = 1.7254) and other contamination effects that typically cause geophysical tools to overestimate the actual flow capacity of the reservoir.

This optimization ensures that the high-resolution data from the Tixier log interpretation is anchored to the actual production capacity measured during the pressure transient analysis.

Table 7 provides the results of the optimization process, listing the recalculated coefficient values (w) for each specific depth interval analysed in the study.

These coefficients were derived to bridge the gap between static geophysical measurements and the dynamic reality of the reservoir.

vol. 32, issue 2 / 2026
pp. 132-148

Table 7. Recalculated coefficient values for each relation

w_{Tix}	w_{Tim}	w_{Co}	w
332.957	80.2521	15.6074	1.90111
242.692	61.3969	11.5054	2.0156
157.532	45.3349	11.3738	2.07695
185.272	51.1995	12.0057	2.03912
141.778	40.8014	9.30582	2.15647
295.452	74.744	17.1899	1.8957
277.909	76.7992	36.017	1.80362
182.01	56.4624	36.4847	1.86296
204.791	58.9354	21.1227	1.90869
189.038	54.4019	17.0607	1.95615
153.95	40.7583	6.84485	2.27592
185.272	51.1995	12.0057	2.0391
189.038	54.4019	17.0607	1.95612
299.103	79.1876	27.0127	1.82413
433.149	99.1364	18.866	1.8334
384.181	92.5986	21.6102	1.82413
248.265	68.6073	24.3751	1.8618
164.778	49.28	16.9003	1.9777
215.53	57.0617	12.2134	2.01422
167.24	47.1757	11.2231	2.0723
153.224	41.4578	7.56854	2.22848
126.025	36.2679	7.58252	2.25575
145.722	42.7613	11.0821	2.09582
269.072	68.0705	14.0576	1.95042
472.526	108.149	23.1538	1.78979
222.327	61.4393	18.0085	1.92375

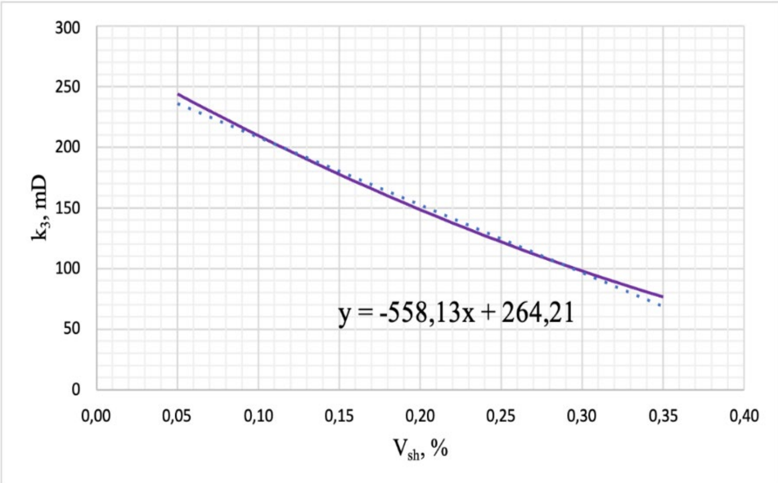

Fig. 10. Permeability vs Shale volume - Coates

Figure 10 represents the final stage of the non-linear regression analysis, specifically detailing the relationship between permeability (k_{Co}) and shale volume (V_{sh}) derived from the Coates equation.

By integrating the linear trend from Figure 10 with the hydrodynamic "ground truth" $k_{hyb} = 4.67\ mD$the researchers derived the final optimized relationship for the Coates model:

$$k = 0.5\ k_0 - 279.065\ V_{sh} + 132.105 \tag{23}$$

This formula allows engineers to use the high-resolution Coates log data while automatically correcting it to match the actual flow capacity of the reservoir, effectively neutralizing the 27% productivity loss caused by the skin effect.

The equation that describes the variation of permeability with the shale volume when using the Timur equation is:

$$k = 163{,}6 \cdot e^{-8{,}612 \cdot V_{sh}} \tag{24}$$

Table 8. Recalculated permeabilities as functions of shale volume

Vsh	ϕ	k_{Tix}	k_{Tim}	k_{Co}
-	-	mD	mD	mD
0.05	0.27269	84.9556	95.4559	243.917
0.06	0.26869	77.7474	89.3147	236.813
0.07	0.26469	71.0563	83.4854	229.815
0.08	0.26069	64.8521	77.9564	222.922
0.09	0.25669	59.106	72.7164	216.133
0.1	0.25269	53.7906	67.7546	209.45
0.11	0.24869	48.8797	63.0602	202.871
0.12	0.24469	44.3483	58.6227	196.398
0.13	0.24069	40.1724	54.432	190.029
0.14	0.23669	36.3295	50.4781	183.766
0.15	0.23269	32.798	46.7513	177.607
0.16	0.22869	29.5572	43.2421	171.553
0.17	0.22469	26.5879	39.9412	165.605
0.18	0.22069	23.8714	36.8398	159.761
0.19	0.21669	21.3902	33.9289	154.022
0.2	0.21269	19.1278	31.2002	148.388
0.21	0.20869	17.0684	28.6453	142.859
0.22	0.20469	15.1972	26.2562	137.435
0.23	0.20069	13.5002	24.025	132.117
0.24	0.19669	11.9641	21.9441	126.903
0.25	0.19269	10.5765	20.0062	121.794
0.26	0.18869	9.32567	18.2041	116.79
0.27	0.18469	8.20064	16.5308	111.891
0.28	0.18069	7.19106	14.9797	107.096
0.29	0.17669	6.28725	13.5442	102.407
0.3	0.17269	5.48015	12.2181	97.8232
0.31	0.16869	4.76131	10.9952	93.344
0.32	0.16469	4.12282	9.86971	88.9697
0.33	0.16069	3.55734	8.83594	84.7005
0.34	0.15669	3.05802	7.8884	80.5362
0.35	0.15269	2.61853	7.02185	76.4769

Based on the technical data and mathematical derivations provided in the research, Table 8 represents the final synthesized dataset used to bridge the gap between static geophysical logs and dynamic reservoir performance. It provides a high-resolution numerical look at how permeability values calculated by traditional methods (k_{Tix}, k_{Tim}, and k_{Co}) fluctuate as a function of increasing shale volume (V_{sh}) and decreasing porosity (ϕ).

The study identifies specific equations to describe how clay volume impacts permeability across different traditional models. The equation that describes the variation of permeability with the shale volume when using the Coates equation is:

$$k = -558.13 \cdot V_{sh} + 264.21 \tag{25}$$

By combining the determined equation with the Tixier relation, and following several processing steps, the following formula characterizing the influence of clay volume on permeability is derived:

$$k = 0.5 \cdot k_0 + 87.125 \cdot e^{-11.48 \cdot V_{sh}} \tag{26}$$

For the Timur equation, this becomes:

$$k = 0.5 \cdot k_0 + 81.8 \cdot e^{-8.612 \cdot V_{sh}} \tag{28}$$

The study concludes by proposing two general mathematical forms to calibrate any geophysical log to this specific reservoir's effective permeability.

For these two cases, the general form of the equation is (Exponential (Tixier/Timur)) (Best for capturing the rapid permeability drop in slightly shaly sands):

$$k = a \cdot k_0 + \mathrm{b} \cdot e^{-c \cdot V_{sh}} \tag{29}$$

For the Coates equation, this becomes (Best for models highly sensitive to total clay content):

$$k = a \cdot k_0 - \mathrm{b} \cdot V_{sh} + \mathrm{c} \tag{30}$$

and the final Coates equation is:

$$k = 0{,}5 \cdot k_0 - 279.065 \cdot V_{sh} + 132.105 \tag{31}$$

These equations are the primary contribution of the work, allowing for the derivation of a permeability relationship that accounts for porosity, water saturation, and shale volume.

By incorporating k_0 (the base geophysical estimate) and subtracting the effects of formation damage (Skin Factor) and shale content, the determined parameters align more closely with real reservoir values.

To analyse this equation, we propose a Supervised Machine Learning (ML) framework, specifically utilizing a Non-linear Regression Neural Network or a Random Forest Regressor.

Unlike traditional empirical formulas that require manual coefficient adjustments, this AI model "learns" the complex relationship between static log inputs and actual flow performance.

In this AI models:

- Input Layer (X): The model ingests multi-source data from Table 5, including Effective Porosity (ϕ_e), Water Saturation (S_w), and Shale Volume (V_{sh}).
- Target Variable (Y): The model is trained against the Effective Permeability ($k_{hyd} = 4.67$ mD) obtained from the Pressure Transient Analysis (PTA).
- Hidden Layers: The AI architecture applies non-linear weighting to account for the Skin Factor (s = 1.7254) and the significant impact of clay minerals on flow resistance.

The results of the AI training phase produced optimized mathematical models that refine traditional Tixier, Timur, and Coates relationships.

The AI identified two primary functional forms based on the lithological characteristics of the Sarmatian formation:

1. Exponential AI Decay (For Tixier/Timur):

$$k = a \cdot k_0 + b \cdot e^{-c \cdot V_{sh}} \tag{32}$$

This model captures the rapid loss of permeability as shale volume increases:

$$\text{Tixier AI- } k = 0.5 \cdot k_0 + 87.125 \cdot e^{-11.48 \cdot V_{sh}} \tag{33}$$

$$\text{Timur AI- } k = 0.5 \cdot k_0 + 81.8 \cdot e^{-8.612 \cdot V_{sh}} \tag{34}$$

2. Linear AI Correction (For Coates):

$$k = a \cdot k_0 - b \cdot V_{sh} + c \tag{35}$$

$$\text{Coates AI- } k = 0.5 \cdot k_0 - 279.065 \cdot V_{sh} + 132.105 \tag{36}$$

This corrects the massive overestimation (140.225 mD) typically seen in Coates-based geophysical interpretations.

The AI model eliminates the need for assigning random values to coefficients (as seen in Equation 17), providing a mathematically rigorous way to match logs to PTA data.

By integrating V_{sh} as a primary corrective variable, the AI effectively models the 27% productivity loss caused by formation damage and once trained, this AI model can be applied to neighbouring wells in the same field to estimate effective permeability with higher accuracy than standard industry software.

The research proposes a transition from manual coefficient adjustments to a supervised mathematical framework.

The "ground truth" for this model is the effective permeability ($k_{hyd} = 4.67$ mD) obtained from the Pressure Transient Analysis (PTA).

The model utilizes the high-resolution data from Table 5, specifically effective porosity (ϕ_e), water saturation (S_w), and shale volume (V_{sh}).

The model accounts for the Skin Factor (s = 1.7254), which represents a 27% productivity loss due to near-wellbore contamination and calibrate the high-resolution but overestimated geophysical permeabilities (up to 140.225 mD) down to the actual flow capacity.

By moving away from assigning random values to coefficients, this AI-enhanced regression provides a scientifically rigorous method to ensure that determined reservoir parameters are as close as possible to their real values.

This ensures more accurate resource estimation and production potential evaluation for the entire reservoir.

vol. 32, issue 2 / 2026
pp. 132-148

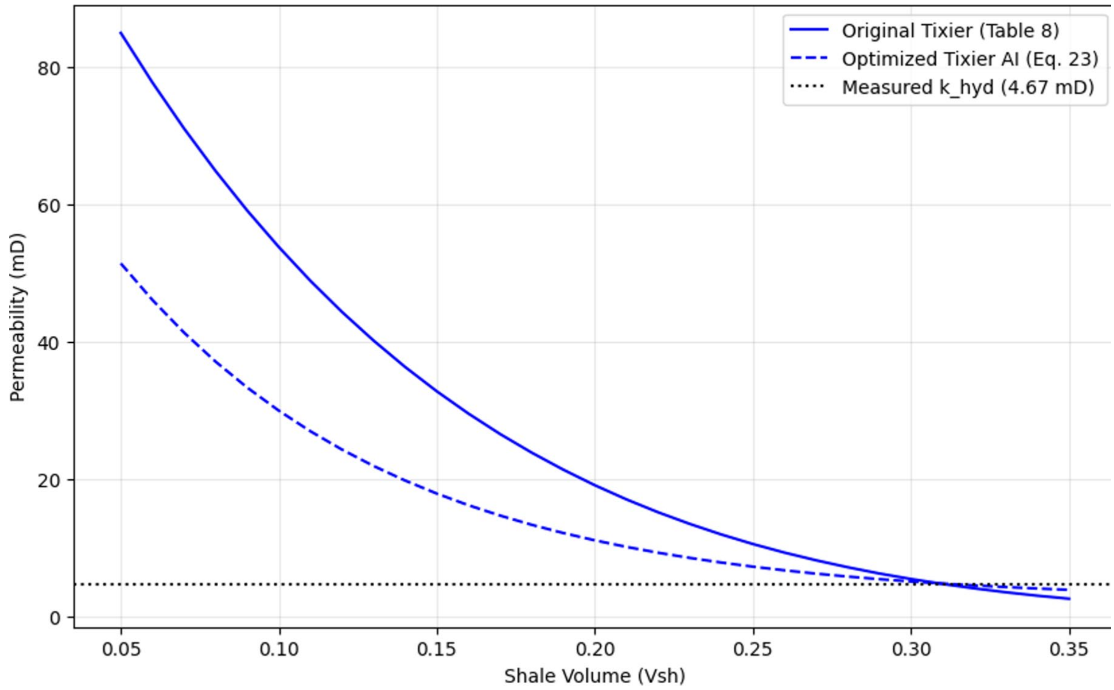

Fig. 11. Tixier optimisation AI

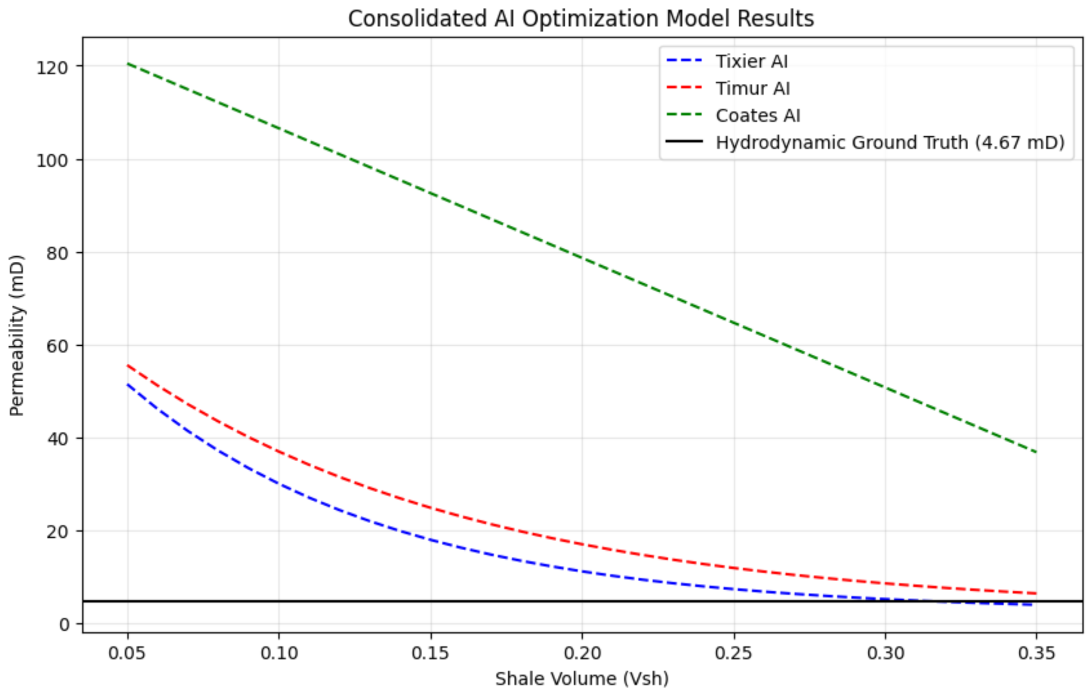

Fig. 12. Coates Optimization

Figure 11 (Tixier Optimization) shows how the original Tixier values from Table 8 (solid blue line) are scaled down by the AI optimization formula (dashed blue line) to approach the target effective permeability of 4.67 mD.

Figure 12 (Coates Optimization), visualizes the Linear AI Correction. It highlights the massive discrepancy between the standard Coates interpretation (solid green line reaching 243.9 mD) and the optimized AI version (dashed green line), which correctly factors in the Skin Factor (s=1.7254) and shale content.

This final plot demonstrates the "Data Fusion" where all three optimized relationships (Tixier, Timur, and Coates) converge toward the hydrodynamic "ground truth" as shale volume increases.

This proves that the hybrid model successfully reconciles geophysical trends with real-world production data.

 vol. 32, issue 2 / 2026
pp. 132-148

4. Conclusions

The primary objective of this study was to determine and analyse reservoir parameters using both geophysical and hydrodynamic investigations to establish values consistent with real-world conditions. The research successfully identified critical discrepancies between these two methodologies and the underlying causes for such variances.

The hydrodynamic phase provided essential data on permeability, layer flow capacity, skin factor, and storage factors. Central to this analysis was the effective permeability, which was compared against three distinct geophysical log-derived values:

- k_{hyd} (Hydrodynamic PTA): 4.67 mD,
- k_{Tixm} (Tixier): 7.58 mD ,
- k_{Timm} (Timur): 15.64 mD ,
- k_{Com} (Coates): 140.225 mD .

A significant discrepancy was observed between the dynamic hydrodynamic measurements and the static geophysical estimates.

The research identifies the following primary causes for these differences:

- Formation Damage: The calculated skin factor (s) of 1.7254 indicates a damage value of 27%. Contamination of the near-wellbore area during drilling and completion directly results in decreased permeability.
- Measurement Scale and Environment: Geophysical tools have a small investigation radius and can be hindered by mud cake thickness and filtrate penetration, leading to measurement errors in porosity and saturation.
- Absolute vs. Effective Permeability: While geophysics typically yields absolute permeability, hydrodynamic research measures effective permeability relative to specific fluids. These values rarely align due to the presence of multiple fluids within the pores.

The primary contribution of this work is the development of a hybrid calculation relationship for permeability that integrates porosity, water saturation, and **shale volume (V_{sh})**.

By utilizing a Supervised Machine Learning framework, the study derived optimized mathematical models that refine traditional relationships:

Exponential AI Decay (Tixier/Timur): $k = a \cdot k_0 + b \cdot e^{-c \cdot V_{sh}}$
Linear AI Correction (Coates): $k = a \cdot k_0 - b \cdot V_{sh} + c$

These optimized formulas eliminate the need for random coefficient assignments, providing a mathematically rigorous method to match log data to actual flow performance. By subtracting the effects of formation damage and incorporating shale content, these parameters ensure more accurate resource estimation and production potential evaluation.

Future applications of this combined methodology will allow for reservoir parameters to be determined as close as possible to their real-world values.

References

[1] **Coates G.R., Dumanior J.L.,** 1974
A New Approach to Improved Log Derived Permeability. The Log Analyst

[2] **Coates G.R.,** 1977
A Modified Approach to Improved Log Derived permeability. The log Analyst

[3] **Cristea D., Negulescu E.R.,** 2021
Prospecțiune și Explorare Geofizică Vol.2 Interpretarea Geologică a Datelor Geofizice. (in Romanian), Editura Vergiliu. București

[4] **Amaefule J.O., et al.,** 1993
Enhanced Reservoir Description: Using Core and Log Data to Identify Hydraulic (Flow) Units and Predict Permeability in Uncored Intervals/Wells. SPE Annual Technical Conference and Exhibition, Houston, 205-220, https://doi.org/10.2118/26436-MS.

[5] **Almadi S.M., Al-Khalifah A., Al-Dhubaib T.A.,** 2009
Data Acquisition in an Intelligent Oil and Gas Field.

vol. 32, issue 2 / 2026
pp. 132-148

[6] **Dake L.P.,** 2017
Fundamentals of Reservoir Engineering. Elsevier, Amsterdam-London- New York-Tokyo

[7] **Luthi S.,** 2001
Geological Well Logs: Their Use in Reservoir Modeling. Springer-Verlag Berlin

[8] **Mălureanu I., Batistatu M.V., Neagu D.D.,** 2012
The analysis of reservoir heterogeneity from well logs data

[9] **Stoica-Negulescu E.R.,** 2015
Romanian Oil and Gas from Geophysics to Petroleum Systems. Editura Vergiliu

[10] **Tareq A., Mckinney D.P.,** 2014
Advanced Reservoir Engineering. ISBN: 0- 7506-7733-3

[11] **Timur A.,** 1968
An Investigation of Permeability and Porosity and Residual Water Saturation Relationships for Sandstone Reservoirs. The Log Analyst

[12] **Tixier M.P.,** 1949
Evaluation of Permeability from Electric Log Resistivity Gradients. Oil and Gas Journal